Chemistry

Physical & Theoretical Chemistry fields

Okayama University *Year* 2004

Bridging the gap between small clusters and nanodroplets: spectroscopic study and computer simulation of carbon dioxide solvated with helium atoms.

Jian Tang* Robert A. McKellar Dr.†

Fabio Mezzacapo‡ Saverio Moroni**

*Okayama University, jtang@cc.okayama-u.ac.jp

†Steacie Institute for Molecular Science

‡Università di Roma La Sapienza

**Università di Roma La Sapienza

Bridging the gap between small clusters and nanodroplets: spectroscopic study and computer simulation of carbon dioxide solvated with helium atoms.

J. Tang,[1] A. R. W. McKellar,[1] F. Mezzacapo,[2] and S. Moroni[2]

[1]*Steacie Institute for Molecular Sciences*
National Research Council of Canada Ottawa, Ontario K1A 0R6, Canada
[2]*SMC INFM, Dipartimento di Fisica, Università di Roma La Sapienza*
Piazzale Aldo Moro 2, I-00185 Rome, Italy

(Dated: November 26, 2003)

High resolution infrared spectra of He_N–CO_2 clusters with N up to about 20 have been studied in the region of the CO_2 ν_3 fundamental band. The B rotational constant initially drops as expected for a normal molecule, reaching a minimum for $N = 5$. Its subsequent rise for $N = 6$ to 11 can be interpreted as the transition from a normal (though floppy) molecule to a quantum solvation regime. For $N > 13$, the B value becomes approximately constant with a value about 17% larger than that measured in much larger helium nanodroplets. Quantum Monte Carlo calculations of pure rotational spectra are in excellent agreement with the measured B in this size range, and complement the experimental study with detailed structural information. For larger cluster size ($N = 30 - 50$) the simulations show a clear sign of convergence towards the nanodroplet B value.

PACS numbers: 61.46.+w, 36.40.Mr, 02.70.Ss

Helium clusters offer the possibility of studying manifestations of superfluidity at a microscopic scale, and more generally effects of confinement in quantum fluids [1]. Superfluidity can be defined and measured in terms of the response to an external perturbation [2, 3]. While Path Integral Monte Carlo calculations found superfluidity behavior in ^{4}He droplets with as few as 64 atoms [4], direct experimental evidence of superfluidity in pure He clusters has remained elusive. In recent years He nanodroplet isolation (HENDI) spectroscopy [5] has made a probe to rotational motion in He droplets available. Spectroscopic interrogation of molecules solvated in ^{4}He droplets reveals free-rotor-like spectra [6], although with an increased moment of inertia. Theoretical descriptions, based on demotion of superfluidity in the first solvation shell induced by the anisotropy and strength of the molecule–He potential [7, 8] and on hydrodynamic response of the modulated superfluid density around the molecule [9], give a fairly good account for the increased moment of inertia observed in large droplets (from a few hundreds to order of ten thousands He atoms), especially for relatively heavy and slow rotors such as SF_6 and OCS. However the relative importance of different effects is still under debate.

Recently, measurements of the evolution of rotational constants with the size of the cluster have been reported [10, 11]. For ^4He_N–OCS, B decreases in the range $N < 8$, undershooting its nanodroplet value, which implies a subsequent turnaround at larger cluster sizes [10]. Quantum Monte Carlo (QMC) calculations of rotational excitations of the cluster confirm the observed undershoot, locating the minimum of B at $N = 6$ [14] or 8–9 [15]. Experimentally, such a turnaround has been observed in ^4He_N–N_2O, with a first minimum of B at $N = 6$, followed by an oscillatory behavior [11]. For N_2O, however, the value of B obtained for all clusters for N up to 12 is significantly above its nanodroplet limit [12]. Slow convergence of B has been predicted for light rotors such as HCN [13], but it is somewhat unexpected for N_2O, which is in several respects similar to OCS. Whether this is related to the anomalously low value of B of the N_2O molecule measured in large droplets [12] is presently not undestood.

In the present paper, we use CO_2 as the probe molecule, and further extend the study of small helium clusters by *(i)* recording infrared spectra in the region of the CO_2 ν_3 fundamental band (2350 cm^{-1}) and *(ii)* calculating the rotational spectrum in the vibrational ground state by means of QMC simulations.

In many respects, CO_2 is similar to N_2O and OCS. But, of course, there is also a significant difference: CO_2 is symmetric and nonpolar. Because of symmetry, only half of the normal rotational levels of ground-state $^{12}C^{16}O_2$ molecules are occupied (odd J-values are forbidden), with the result that He_N-CO_2 cluster spectra are simpler and less congested than those of He_N-N_2O and He_N-OCS. But these missing rotational transitions also mean that the spectra contain less information. The net effect is that we can more easily follow the pattern of He_N-CO_2 transitions to high N–values ($N = 18+$, which is considerably higher than for He_N-N_2O and He_N-OCS), but the resulting rotational assignment and analysis is less secure and precise. While confirmation of infrared assignments from observations of analogous pure rotational microwave transitions is not possible for CO_2 as it was for N_2O and OCS, the agreement with the theoretical simulations reported here strongly support the experimental analysis.

The apparatus was similar to that used previously in our work on He clusters [10, 16]. A tunable infrared diode laser is used to probe a pulsed supersonic jet expansion. The gas mixtures consist of very small concentrations (0.1 to 0.002%) of CO_2 in ultra–high purity helium. We use both pinhole– and slit–shaped jet nozzles, with temperatures varied from -20 to -160 °C, and rather high backing pressures up to about 45 atm. The N-value assignments were primarily based on the order in which the lines appear as clustering is increased in the supersonic expansion by raising backing pressure and lowering jet temperature. The assignments were also supported by

the rotational analyses, as described below. Finally, they were partly based on achieving a smooth behavior of line position as a function of N.

Details of the assignments will be reported elsewhere [17]. We discuss here the rotational analysis. Three transitions, $R(0)$, $P(2)$, and $R(2)$, were assigned for each cluster with N between 3 and 17 [18]. These limited data can be fitted in terms of at most three parameters. The only practical approach is to use the simple linear molecule energy expression, $E = \nu_0 + BJ(J+1) - D[J(J+1)]^2$, to determine the band origin, ν_0, rotational constant, B, and centrifugal distortion constant, D, assuming that B and D are the same in the ground and excited vibrational states, $\nu_3(CO_2)$=0 and 1.

The variation of the vibrational band origin, ν_0, with cluster size is shown in Fig. 1(a), which includes a comparison with He$_N$–OCS and He$_N$–N$_2$O. All three cluster systems show the same turnaround in vibrational shift at $N = 5$, which can be explained by the donut model in which the first five He atoms occupy equivalent positions around the equator of the CO_2, OCS, or N_2O, where each exerts a similar blue-shifting effect. Subsequent He atoms occupy positions closer to the ends of the molecule, where they exert a red-shifting effect on the vibration. The very close match between the CO_2 and OCS shifts for $N = 1$ to 8 in Fig. 1(a) is quite remarkable, and this helps to support the present analysis for $N = 3$ to 8. Unfortunately, we cannot compare the present vibrational shifts with that of CO_2 in helium nanodroplets since our observations were in the ν_3 fundamental band region, while the only available nanodroplet observations apply to the ν_1+ν_3 and $2\nu_2$+ν_3 bands [12].

The variation of B rotational constant with N is shown in Fig. 1(b). Starting at the value for the isolated CO_2 molecule, 0.39 cm^{-1}, B drops to a minimum of 0.11 cm^{-1} at $N = 5$, and then rises through a broad local maximum of 0.20 cm^{-1} around N = 11, signaling a transition to a regime where a fraction of the helium density is decoupled from the rotation of the molecule [11, 14, 15]. For $N = 14$ to 17, B decreases slightly to an almost constant value of 0.18 cm^{-1}. The limiting large-N value for helium nanodroplets [12], $B = 0.154$ cm^{-1}, is indicated by a dashed line in Fig. 1(b), and it appears that this value will be approached from above as N goes from 17 to 5000. For He$_N$-OCS, B decreases steadily from $N = 0$ to 8, passing through the nanodroplet value at about N = 5, and its eventual turnaround has not yet been observed experimentally [10]. For He$_N$-N$_2$O, the variation of B is rather similar to that of He$_N$-CO_2, but with the significant difference that B always remains above its nanodroplet value for He$_N$-N$_2$O [11]. The He$_N$-CO_2 and He$_N$-N$_2$O rotational parameters are almost identical for $N = 1$, 3, 4, and 5. A significant deviation starts for $N = 6$, where the B value of He$_N$-CO_2 rises while that of He$_N$-N$_2$O continues to fall [11]. It is tempting to relate this difference to symmetry: the donut ring having been filled with five He atoms, the sixth atom can go to the preferred end of N_2O. But has no such easy choice with CO_2, where it must divide itself between the two ends. This has the effect of destabilizing the ring. Evidently, the OCS, N_2O, and CO_2 molecules behave rather differently in small helium clusters in spite of their close family ties, as already known for larger clusters from HENDI spectroscopy [12]. In general terms, the fact that He$_N$-CO_2 shows the earliest and most pronounced B value turnaround, compared to the other family members, is not surprising in view of its higher symmetry and the weaker anisotropy of its interaction with helium [20–22].

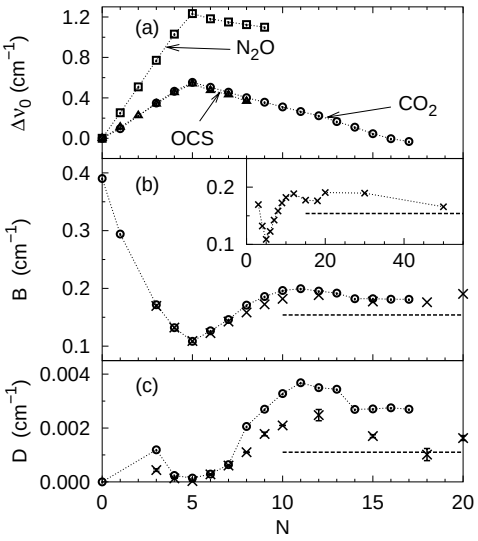

FIG. 1: Variation with the cluster size of (a) the vibrational band origin, $\Delta\nu_0$, (b) the rotational constant, B, and (c) the centrifugal distortion constant, D. Circles and crosses indicate respectively the present experimental and theoretical results for He$_N$–CO_2. Panel (a) includes for comparison the value of $\Delta\nu_0$ for He$_N$–OCS [10] and He$_N$–N$_2$O [11]. The inset of panel (b) shows the calculated B–values in an extended range. The dashed lines indicate the nanodroplet results [12].

Figure 1(c) shows the variation with N of the centrifugal distortion parameters, D. We can compare these values with those determined previously for He$_N$-OCS and He$_N$-N$_2$O clusters [10, 11]. The He$_N$-OCS distortion parameters are considerably smaller, while those of He$_N$-N$_2$O are mostly smaller but fairly similar to those of He$_N$-CO_2 for $N = 3$ to 7. This is consistent with the fact that He–CO_2 intermolecular forces [20] are significantly weaker than those for He–N$_2$O [22]. But it is not so easy to understand why the He$_N$–N$_2$O distortion parameters are significantly larger than those of He$_N$–OCS, since the depth of the intermolecular potential well is smaller in the latter case [21]. Overall, we can say that the similarity between He$_N$-CO_2 and He$_N$-N$_2$O distortion parameters for $N = 3$ to 7 tends to support the present analysis; some other possible assignments would give much less reasonable D values. For $N = 8$ and larger, the present D values jump into the range 0.0020–0.0035 cm^{-1}, which is quite large compared to He$_N$-N$_2$O [11], or to CO_2 in nanodroplets [12], both of which have $D \approx 0.001$ cm^{-1}. In defense of these large D values, we can make the following points. First, we do expect very floppy behavior because of the weak He–CO_2 intermolecular forces. Second, the present experimental D values may not be so meaningful because of the sparse nature

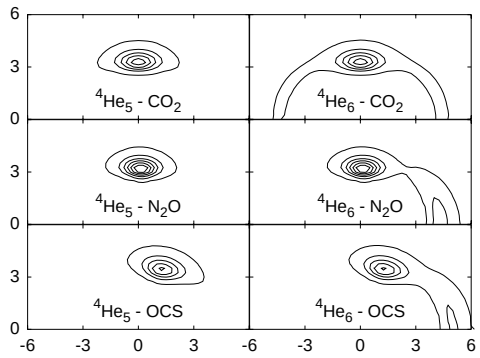

FIG. 2: Contour plot of the helium density profile in a plane containing the molecular axis, for clusters of 5 and 6 helium atoms. The molecule (either CO_2, N_2O [26], or OCS [27]), has its center of mass at the origin and an oxygen atom on the positive x directon. Distances are in Angstrom, and contour levels start at 0.002 with increments of 0.010, in units of inverse cubic Angstrom.

of the data and the simple three parameter fits. If more data were available and higher order distortion and vibrational dependence of B and D were included, then the D values might change significantly. And third, other reasonable assignment schemes that we tried resulted in similarly large D values.

We turn now to the presentation of the QMC calculation. The simulations are performed with the reptation QMC algorithm [23], using recent *ab initio* results for both the He–He interaction [24] and the He–CO_2 potential energy surface (PES) in the vibrational ground state of the molecule [20]. Details of the simulations are similar to those of Ref. [15] and need not be repeated here. The estimates of the ground state energy of the clusters and the He density profiles $\rho(\mathbf{r})$ are exact, for given interparticle interactions, within known statistical errors. The calculation of the rotational spectrum is less straightforward. For a cluster with a given N, the simulation gives unbiased estimates for the imaginary-time correlation functions $c_J(\tau) = \langle P_J(\mathbf{n}(\tau)\cdot\mathbf{n}(0))\rangle$, where $P_J(\cos(\theta))$ are Legendre polynomials, $\mathbf{n}(\tau)$ is the versor of the molecular axis at imaginary time τ, and $\langle\ \rangle$ denotes a ground state average. The energies of the eigenstates of the cluster with total angular momentum J, involving molecular rotation, are then obtained from a fit to $c_J(\tau)$ [15]. Finally, excitation energies at different values of J are analyzed in terms of a linear rotor model, yielding the rotational constant B and the distortion parameter D. The analytic continuation of imaginary time correlation functions is in general an ill-conditioned problem [25]. However the experimental observation that the rotational spectrum of the cluster is well represented by a free linear rotor implies that for given J there is a strong peak well separated in energy from other spectral features. In these conditions, the position of the peak inferred from imaginary time correlations is fairly robust against details of the fitting procedure. Success of a similar analysis for He$_N$–OCS and He$_N$–N_2O clusters [15, 26] further supports the reliability of the procedure.

The He density profiles for He$_N$–CO_2 clusters with $N = 5$ and 6 are compared in Fig. 2 with those of He$_N$–OCS [27] and He$_N$–N_2O [26]. The structural information (donut model) contained in the turnaround of the measured vibrational shift at $N = 5$ for all these clusters is clearly demostrated: the first five atoms fill an equatorial ring around the molecule, and the sixth spills out towards the poles of the molecule, leaving the density in the ring essentially unchanged. For He$_6$–CO_2 the density outside the donut is evenly distributed, owing to both the symmetry and the shape of the PES (for CO_2, secondary minima of the potential at the molecular poles are shallower than for OCS [21] or N_2O [22] on the oxygen side). The effect of the sixth atom in destabilizing the ring, experimentally observed as a reduction of the moment of inertia, can be characterized in terms of the molecule–atom angular motion correlation $\phi(\mathbf{r}) = -\langle \mathbf{L}\cdot\mathbf{l}(\mathbf{r})\rangle$, where $\mathbf{L}$ indicates the angular momentum of the CO_2 molecule, and $\mathbf{l}(\mathbf{r})$ is the angular current operator of He atoms at point $\mathbf{r}$ [15]. A large value of $\phi(\mathbf{r})$ means that the local He density tends to follow the molecular rotation. We find that for the He$_6$–CO_2 cluster $\phi(\mathbf{r})$ is zero, within statistical noise, outside the ring, and significantly lower than for $N = 5$ in the donut region. Therefore the "wings" of density which appear for $N = 6$ do not give any local contribution to the moment of inertia; furthermore their presence has the effect of decoupling from molecular rotation some of the density present in the donut region (making permutation cycles with a large projected area more likely [8]). For He$_6$–OCS and He$_6$–N_2O, on the other hand, localization of the density in the polar angular coordinate accounts for the observed increase of the moment of inertia from $N = 5$ to 6 [10, 11].

Further structural information is obtained from the ground state energy of the clusters, $E(N)$. Fig. 3 shows the incremental binding energy per added He atom, $E(N) - E(N-1)$ (approximated as $[E(N_i) - E(N_j)]/(N_i - N_j)$ when simulations for consecutive values of N have not been done). Once again, the fact that the first five He atoms occupy equivalent positions is manifest. Also clear, both in the incremental binding energy and in the radial distribution $r^2\rho(r)$ of the He density, shown in the inset of Fig. 3, is the signature of the first solvation shell completion before $N = 20$.

Finally we compare in Fig. 1(b),(c) the measured and calculated values of the rotational constant B and centrifugal distortion D. For all the cluster sizes where both experimental and theoretical values have been determined, the agreement for B is almost perfect –the main difference being a small theoretical underestimate of the broad maximum around $N = 11$. Note that the simulations for N up to 15 were performed without prior knowledge of the experimental results. The calculated centrifugal distortions are generally smaller than those obtained from the rotational analysis of the measured spectra. However both the general trend of the dependence on the cluster size, and the very large value of D compared to the OCS– and N_2O–doped cluster, are well reproduced. In view of the uncertainties inherent in a rotational analysis with rather sparse data, we consider the overall agreement quite gratifying. For larger cluster sizes, the theoretical value of

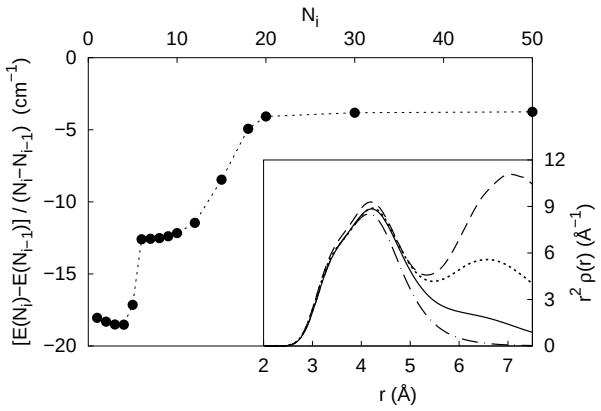

FIG. 3: Incremental binding energy per added helium atom for He_N–CO_2 clusters (top and left scales). Statistical errors are smaller than the symbol size. The inset shows the radial distribution of the He density (bottom and right scales) for $N = 15$ (dash–dotted line), 20 (solid), 30 (dotted) and 50 (dashed).

the rotational constant rises again at $N = 20$, corresponding to completion of the first solvation shell, and (assuming one can interpolate smoothly between rather distant values of N) begins to approach the nanodroplet limit by $N = 50$.

In summary we have determined the effective rotational constant B of He_N–CO_2 clusters using both high resolution infrared spectroscopy and computer simulation. We stress the impressive agreement obtained with completely independent experimental and theoretical methods. The main feature to emerge is the B–value turnaround at $N = 5$, earlier (lower N), sharper, and more dramatic than in He–N_2O and He_N–OCS. We conclude with a few comments on the results reported. First, the quality of the He–CO_2 PES [20] employed here is quite remarkable. This suggests that measurements and simulations of medium–large size clusters can be useful in general to gauge the accuracy of PES, and should motivate accurate calculations of helium–molecule interactions in vibrationally excited states for reliable theoretical studies of vibrational shifts. Second, lacking confirmation from pure rotational microwave transitions for CO_2, the present infrared line assignments were partly based on assumptions such as the smooth behavior as a function of N and the independence of the rotational constants on the vibrational state of the molecule. The excellent agreement with the completely independent simulation results supports these assumptions and gives confidence in the assignments. Third, the experimental determination of the rotational constant, up to a number of helium atoms close to completion of the first solvation shell, gives a value still significantly higher than its nanodroplet limit. This extends to larger cluster sizes (and QMC simulations push even further) a similar result previously observed in He_N–N_2O [11], suggesting that a nontrivial evolution of the B value beyond the first solvation shell might be a rather common property.

We thank G. Scoles and S. Baroni for stimulating discussions.

[1] S. A. Chin and E. Krotscheck, Phys. Rev. B **52**, 10405 (1995).

[2] G. Baym, in *Mathematical Methods in Solid State and Superfluid Theory*, edited by R. C. Clark and E. H. Derrick (Oliver and Boyd, Edinburgh, 1969), p. 121.

[3] E. L. Andronikashvili, J. Phys. (Moscow) **10**, 201 (1946).

[4] P. Sindzingre, M. L. Klein, and D. M. Ceperley, Phys. Rev. Lett. **63**, 1601 (1989).

[5] C. Callegari, K. K. Lehmann, R. Schmied and G. Scoles, J. Chem. Phys. **115**, 10090 (2001).

[6] S. Grebenev, J. P. Toennies and A. F. Vilesov, Science **279** 2083 (1998).

[7] Y. Kwon, P. Huang, M. V. Patel, D. Blume and K. B. Whaley, J. Chem. Phys. **113**, 6469 (2000).

[8] E. W. Draeger and D. M. Ceperley, Phys. Rev. Lett. **90**, 065301 (2003).

[9] C. Callegari *et al.*, Phys. Rev. Lett. **83**, 5058 (1999).

[10] J. Tang, Y. Xu, A. R. W. McKellar, and W. Jäger, Science **297**, 2030 (2002); Y. Xu and W. Jäger, J. Chem. Phys. **119**, 5457 (2003); J. Tang and A. R. W. McKellar, *ibid.*, p. 5467.

[11] Y. Xu, W. Jäger, J. Tang, and A. R. W. McKellar, Phys. Rev. Lett. **91**, 163401 (2003).

[12] K. Nauta and R. E. Miller, J. Chem. Phys. **115**, 10254 (2001).

[13] A. Viel and K. B. Whaley, J. Chem. Phys. **115**, 10186 (2001).

[14] F. Paesani, A. Viel, F. A. Gianturco, and K. B. Whaley, Phys. Rev. Lett. **90**, 073401 (2003).

[15] S. Moroni, A. Sarsa, S. Fantoni, K. E. Schmidt, and S. Baroni, Phys. Rev. Lett. **90**, 143401 (2003).

[16] J. Tang and A. R. W. McKellar, J. Chem. Phys. **119**, 754 (2003).

[17] J. Tang and A. R. W. McKellar, to be published.

[18] The binary complex, He–CO_2, was studied previously: M.J. Weida, J.M. Sperhac, D.J. Nesbitt, and J.M. Hutson, J. Chem. Phys. 101, 8351 (1994).

[19] J. Tang and A.R.W. McKellar, J. Chem. Phys. **117**, 2586 (2002).

[20] T. Korona, R. Moszynski, F. Thibault, J.-M. Launay, B. Bussery-Honvault, J. Boissoles, and P.E. Wormer, J. Chem. Phys. 115, 3074 (2001).

[21] J. M. M. Howson and J. M. Hutson, J. Chem. Phys. **115**, 5059 (2001).

[22] (a) B. T. Chang, O. Akin-Ojo, R. Bukowski, and K. Szalewicz, J. Chem. Phys. **119**, 11654 (2003); (b) X. Song, Y. Xu, P. N. Roy, and W. Jäger (to be published).

[23] S. Baroni and S. Moroni, Phys. Rev. Lett. **82**, 4745 (1999).

[24] T. Korona, H. L. Williams, R. Bukowski, B. Jeziorski and K. Szalewicz, J. Chem. Phys. 106, 5109 (1997).

[25] J. E. Gubernatis and M. Jarrell, Phys. Rep. **269**, 135 (1996).

[26] S. Moroni, N. Blinov, P. N. Roy, to be published.

[27] For OCS dopant, $\rho(r)$ is calculated with the *unmorphed* version of the PES of Ref. [21]. Morphing the potential causes some of the He density to leak on the sulfur side [15] for $N = 6$. Using the unmorphed PES we find significantly better agreement with the experimental value [10] of B for $N > 5$.